Lab on a Chip

FOCUS

View Article Online
View Journal | View Issue

Cite this: *Lab Chip*, 2015, **15**, 2352

DOI: 10.1039/c5lc90047f

www.rsc.org/loc

Nano-photocatalysts in microfluidics, energy conversion and environmental applications

Jemish Parmar,[a] Seungwook Jang,[b] Lluís Soler,[c] Dong-Pyo Kim[b] and Samuel Sánchez*[ade]

Extensive studies have been carried out on photocatalytic materials in recent years as photocatalytic reactions offer a promising solution for solar energy conversion and environmental remediation. Currently available commercial photocatalysts still lack efficiency and thus are economically not viable for replacing traditional sources of energy. This article focuses on recent developments in novel nano-photocatalyst materials to enhance photocatalytic activity. Recent reports on optofluidic systems, new synthesis of photocatalytic composite materials and motile photocatalysts are discussed in this article.

The development of microfluidic reactors for photocatalytic applications presents valuable advantages like simultaneous and fine control of light and fluids, large surface area-to-volume ratio and uniform distribution of light onto the photocatalyst. Several groups have used microfluidic chips for enhanced chemical reaction performance.[1] The synergy of combining optofluidics and photocatalysis could boost photocatalytic reaction rates and yields, due to an improvement of the mass and photon transfer in the microfluidic reactors.[2] Recent research with non-titania based novel active nano-photocatalysts and titania based novel photocatalytic systems are discussed in this article. The employment of novel nano-photocatalysts is a promising approach for the development of photocatalytic reactors for multiple applications such as solar energy conversion and photodegradation of organics. We expect the field of nano-photocatalytic systems will grow substantially in the near future.

Microfluidics

Optofluidics, which combines microfluidics and optics has become a promising platform for photocatalytic reactions due to short light travel distance within the microchannels. Optofluidic systems increase photocatalytic reaction rate because of the improved mass and photon transfer efficiency. Development of novel photocatalysts and screening of the optimal conditions to study mechanisms and kinetics is challenging due to expensive and bulky setup. Conventional experiments typically require large scale volume setups with

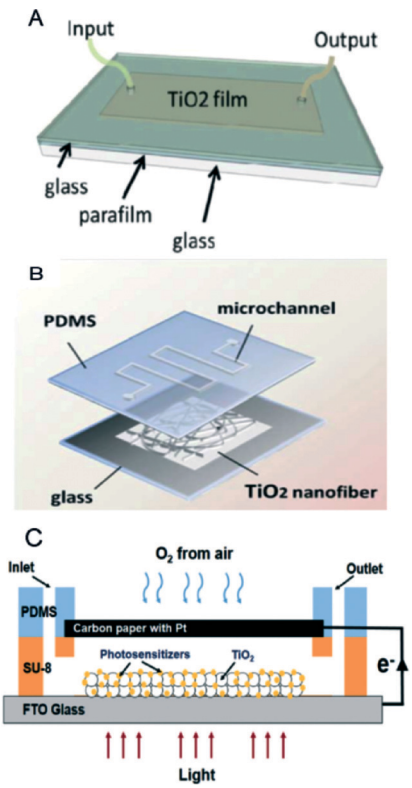

Fig. 1 Various types of optofluidic microreactors. (A) Scheme and photograph of thin TiO_2 film coated planar microreactor. (B) Scheme of nanofibrous TiO_2 microreactor. (C) Schemes and working principle of μ-PFC microreactor. Reprinted from ref. 3 (A), ref. 4 (B) and ref. 5 (C) with permission.

[a] *Max-Planck Institute for Intelligent Systems, Heisenbergstr. 3, 70569 Stuttgart, Germany. E-mail: sanchez@is.mpg.de, ssanchez@ibecbarcelona.eu*
[b] *National Center of Applied Microfluidic Chemistry, Department of Chemical Engineering, POSTECH (Pohang University of Science and Technology), Pohang, Korea 790-784*
[c] *Institute of Energy Technologies, Universitat Politècnica de Catalunya, Diagonal 647, 08028 Barcelona, Catalonia, Spain*
[d] *Institute for Bioengineering of Catalonia (IBEC), Baldiri I Reixac 10-12, 08028 Barcelona, Spain*
[e] *Institució Catalana de Recerca i Estudis Avançats (ICREA), Psg. Lluís Companys, 23, 08010 Barcelona, Spain*

catalysts containing precious metals. Miniaturized reactor space in a microreactor can minimize labour force, cost of experiment and allow for rapid optimization of reactions. Ahsan *et al.* used a microfluidic platform to study the kinetics of photocatalytic water-splitting.[3] They used a planar type PDMS reactor with glass to maximize the light exposure area (Fig. 1A). Pt–TiO_2 photocatalyst was synthesized by sol–gel reaction and the prepared colloidal suspension was spread on the glass substrate. O_2 and H_2 were evolved by Z-scheme system with redox mediators. The reaction rates for O_2 and H_2 were measured under different flow rates and concentrations of mediator. It was observed that the reaction efficiency was clearly improved with increasing flow rate due to enhanced mass transport. Especially higher flow rates would yield 2-fold improved reaction rates.

Meng *et al.* reported a novel microfluidic-based photocatalytic microreactor by using nanofibrous TiO_2 as a photocatalyst with a simple fabrication process and high photocatalytic efficiency.[4] The nanofibrous TiO_2 catalyst was produced by electrospinning and calcination process with high BET surface area (20.8 m^2 g^{-1}). The prepared nanofibrous TiO_2 was transferred and sealed between a PDMS mold and glass substrate (Fig. 1B). The photocatalytic activity of the nanofibrous TiO_2 microreactor was compared with the TiO_2 film microreactor by measuring methylene blue (MB) photodegradation. The investigation of photocatalytic activity with different flow rates revealed that the MB degradation reaction rate was increased sharply with an increase in residence time. The highly porous structure of nanofibrous TiO_2 provides a large surface area while the TiO_2 film reactor only provides limited contact area. The nanofibrous TiO_2 microreactor has a higher efficiency of photocatalytic reaction than that of bulk and film microreactors.

Li *et al.* proposed a micro-photocatalytic fuel cell (μ-PFC) with membrane-free and air-breathing modes.[5] As shown in Fig. 1C, the μ-PFC was designed by fabricating PDMS and a carbon paper with Pt on the TiO_2 film deposited FTO glass. As compared to traditional PFCs, μ-PFCs with a shorter distance between the electrodes along with the membrane can decrease the mass/photon transfer resistance, resulting in enhanced electricity generation. Furthermore, the air-breathing cathode can supply O_2 from the surrounding air with intrinsic large surface to volume ratio, which provides a simple and compact structure as compared to conventional PFCs. The μ-PFCs achieved high performance with 0.58 mW cm^{-2} of maximum power density and a degradation efficiency of 83.9%. This new type of μ-PFC brings in the possibility of promising applications like degrading pollutants and generating electricity.

Energy conversion and environmental applications

Dinh *et al.* described a visible light activated photocatalyst based on nanostructured Au/TiO_2.[6] They fabricated a three-dimensional ordered assembly of thin-shell Au/TiO_2 hollow nanospheres (Au/TiO_2 3DHNSs) that showed higher photocatalytic activity under visible light than conventional Au/TiO_2 nanopowders. The authors also investigated the optical and photocatalytic properties of the Au/TiO_2 3DHNSs structure. Analyzing the reflection and absorption spectra of the samples, the authors concluded that the particular architecture of the photocatalyst plays a key role in enhancement of visible light absorption. The wavelength overlapping between surface plasmon resonance of Au NPs at 580 nm and the photonic stop band in the range 550–620 nm (Fig. 2A) produces an enhanced light harvesting effect. It is known that photons with wavelengths near to the stop band edges can be slowed down and propagate in the material with strong low group velocities through an effect called the slow photon effect.[7] When the wavelength of the slow photon overlaps

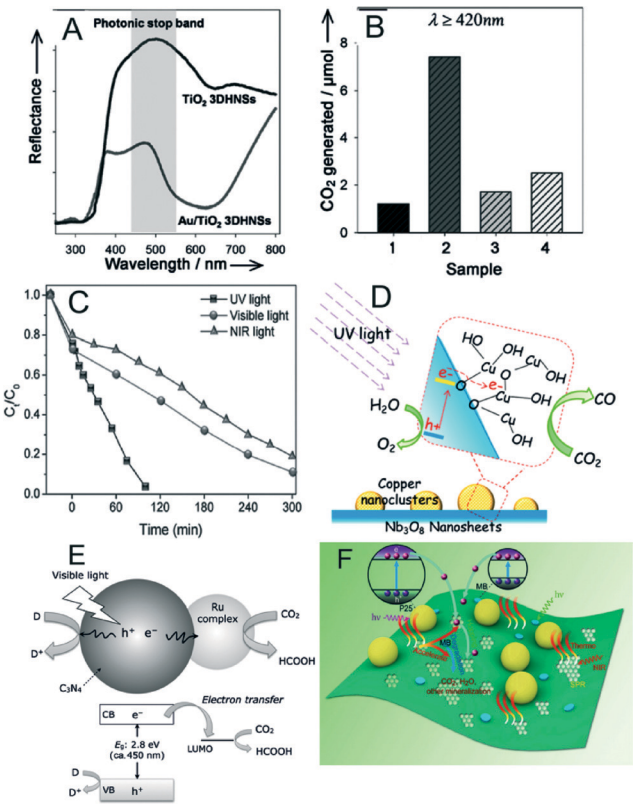

Fig. 2 (A) Diffuse reflectance UV-vis spectra for Au/TiO_2 3DHNSs and TiO_2 3DHNSs as a reference sample. The shaded area in (A) illustrates the presence of the photonic stop band. (B) Generation of CO_2 under visible light illumination ($\lambda \geq 420$ nm) for 10 h using (1) Au/TiO_2-P25, (2) Au/TiO_2 3DHNSs, (3) crushed Au/TiO_2 3DHNSs, (4) Au/TiO_2-HNSs (without the 3D ordered structure) as photocatalysts. (C) Photocatalytic degradation of methyl orange (MO) solution in the presence of WS_2 nanosheets under UV, visible and NIR light irradiation. (D) Schematic of the CO_2 photoreduction to CO using Cu(II) nanoclusters grafted onto $Nb_3O_8^-$ nanosheets. (E) Schematic of the CO_2 photoreduction to formic acid using a Ru complex/C_3N_4 hybrid photocatalyst. CB and VB stand for conduction band and valence band, respectively. (F) Photocatalytic, photothermal and electron shuttling effect in the nanocomposite of P25 attached rGO. Reprinted from ref. 6 (A, B), ref. 8 (C), ref. 9 (D), ref. 10 (E) and ref. 11 (F) with permission.

with the specific absorption of the material, the enhancement of the absorption can occur as a result of increased interaction between slow photons and the material. Their results showed that, besides the slow photon effect, the multiple light scattering caused by the Au/TiO_2 3DHNSs is also important for the enhancement of UV/Vis light absorption. The photocatalytic activity tests of Au/TiO_2 3DHNSs to photodegrade isopropanol to carbon dioxide (CO_2) under visible light revealed that Au/TiO_2 3DHNSs produced 6.1 times more CO_2 than conventional Au/TiO_2-P25 Degussa nanopowder (Fig. 2B).

Sang *et al.* reported the application of tungsten disulfide (WS_2) nanosheets as an efficient photocatalyst capable of photodegrading organic dyes under UV, visible and NIR light.[8] The authors performed a pyrolytic synthesis of the WS_2 nanosheets decomposing $(NH_4)_2WS_4$ at 1200 °C in a H_2 flow. The authors examined the photocatalytic degradation of methyl orange (MO) and Rhodamine B (RhB) in aqueous solutions, preparing suspensions of WS_2 nanosheets with the model contaminated waters and irradiating the suspensions with UV, visible and NIR light. As illustrated in Fig. 2C, MO present in the aqueous solution was fully degraded after 100 min under UV light irradiation, *ca.* 90% of MO was degraded after 300 min of visible light irradiation and *ca.* 80% of MO was degraded after 300 min under NIR light, showing the full-spectrum photocatalytic activity of WS_2 nanosheets. The optimum photocatalytic activity was found at pH 2. The robustness of the WS_2 photocatalyst was demonstrated with up to five consecutive runs of photodegradation of MO in solution under NIR light irradiation, observing a similar activity in all the experiments.

Earlier this year, Yin *et al.* grafted copper oxide (Cu(II)) nanoclusters onto $Nb_3O_8^-$ nanosheet light harvesters as an efficient photocatalyst for the reduction of CO_2 to carbon monoxide (CO).[9] $Nb_3O_8^-$ nanosheets were synthesized using a previously described method.[12] The authors observed effective CO generation (*ca.* 1.4 μmol in 20 h of reaction) on irradiating the photocatalyst with UV light under CO_2 atmosphere. Based on the obtained results of the characterization of the Cu(II)-grafted $Nb_3O_8^-$ nanosheets, the authors suggested the photocatalytic process depicted in Fig. 2D. Irradiation of UV light generates electrons and holes in the conduction and valence bands, respectively, of the $Nb_3O_8^-$ nanosheets. Then, the electrons are transferred into the Cu(II) nanoclusters, where CO_2 is reduced to CO. Simultaneously, the holes in the valence band oxidize water to generate oxygen molecules.

Almost at the same time, parallel efforts of Kuriki *et al.* reported the synthesis of a heterogeneous photocatalyst using carbon nitride (C_3N_4) and a ruthenium (Ru) complex capable of reducing CO_2 into formic acid under irradiation of visible light.[10] Detailed methods of preparation of graphitic C_3N_4 with 12 nm mesopores and Ru complexes suitable for photocatalytic CO_2 reduction were reported previously.[13,14] The authors proposed the photocatalytic mechanism illustrated in Fig. 2E. C_3N_4 is employed as a visible light harvesting unit, generating electrons and holes in the conduction and valence bands, respectively. The generated electrons are injected into the Ru complex, which hosts the active site for CO_2 reduction. Therefore, the photocatalytic efficiency of the present system depends on the structure of the Ru complex. The experimental results testing different Ru complexes on the photocatalytic reduction of CO_2 showed that the best efficiencies were obtained when the complex *trans*(Cl)-[Ru(bpy-$(PO_3H_2)_2$)$(CO)_2Cl_2$] was used to functionalize the C_3N_4 light harvesting material.

Enhanced photocatalytic activity is required to harvest the maximum energy of light and to make photocatalytic systems economically viable. Zhixing Gan *et al.* studied the role of photothermal contributions in enhanced photocatalytic activity of graphene based nanocomposite materials.[11] Photothermal effects in graphene based material are mainly produced by surface plasmons. It shows relatively stronger oscillation of plasmons compared to other 2D materials. Plasmons of rGO cause oscillation of Dirac fermions like electrons in graphene islands and collective oscillations of electrons in graphene remain confined in the structure, which produce local heat. In order to quantify the photothermal contribution, the authors used P25-rGO nanocomposite. TEM analysis revealed that P25(TiO_2) nanoparticles with diameters of approximately 20 nm were attached to the rGO sheet. The authors used MB as a model pollutant to study the enhancement of degradation. Briefly, two sets of experiments with UV-vis light and NIR light were performed for MB degradation using P25 and P25-rGO. After 30 minutes of irradiation, variation in adsorbed mass of MB on rGO was calculated by TGA and variation in mass in the solution was calculated from degradation rate. Based on the temperature increment during experiments and MB degradation rate ratio between P25-rGO and P25, the authors calculated that PTE contribution by rGO in enhanced degradation of MB can be up to 37.5%. Overall enhancement of degradation can be described by mainly three effects, improved light absorption, trapping and shuttling of electrons and a local photothermal effect caused by surface plasmon resonance under NIR exposure (Fig. 2F).

Light activated mobile nanocatalysts

Mass transfer over the surface of heterogeneous photocatalysts is important for higher catalytic degradation. Dunpu Zhang *et al.* fabricated motile photocatalyst film inspired by biological cilia, which can be actuated by an external magnetic field (Fig. 3A).[15] Compared to planar photocatalysts, the ciliary structure provides a higher surface area for the reaction and light absorption while motion makes it capable of transferring mass at the nano and micrometer scale. Artificial cilia were fabricated by self-assembly of cobalt particles suspended in PDMS polymer under a perpendicular magnetic field (900 mT). Thereafter, a TiO_2 film was grown on top of it *via* a hydrothermal synthesis process in a Teflon lined autoclave. In the final step graphene was reduced using UV light

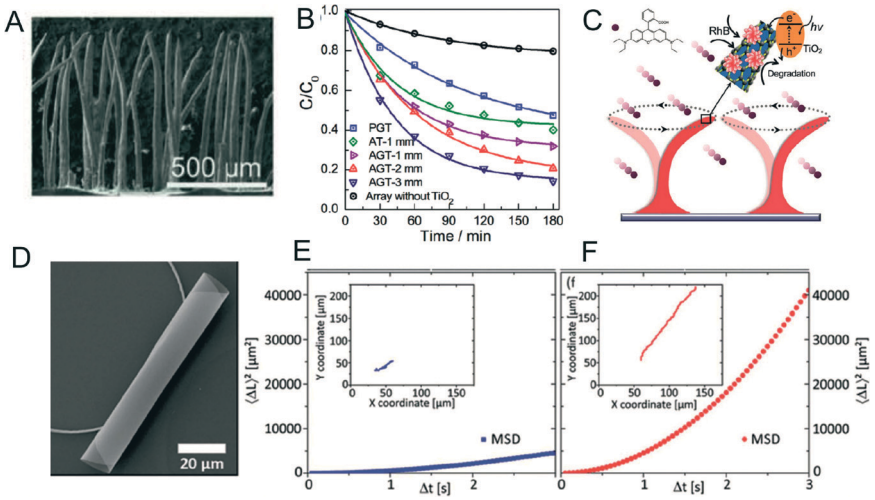

Fig. 3 (A) SEM image of artificial cilia-like structures. (B) Rhodamine B photocatalytic degradation curve by artificial cilia with TiO_2 (AT), planar structure (PGT) and artificial cilia with graphene and TiO_2 (AGT). (C) Schematic of mechanism of mass transfer with ciliary beats and photocatalytic degradation of RhB. (D) SEM image of a TiO_2 rolled up microtube. (E) and (F) show the mean square displacement without and with UV light exposure. Reprinted from ref. 15 (A–C) and ref. 16 (D–F) with permission.

irradiation. Here, graphene was used to provide high conductivity to increase the lifetime of the electron–hole pair. By mimicking ciliary motion using an external magnetic field and controlling beat frequency, artificial cilia can efficiently perform fluid mixing. Mixing enhances the mass transfer process. RhB was used as a model to study the photocatalytic performance and the measurements for degradation rate were carried out using a UV-vis spectrometer. The authors observed that ciliary structures outperformed planar structures in the photocatalytic degradation experiment (Fig. 3B). Enhanced photocatalytic activity can be attributed to micromixing capability, higher light absorption and higher surface area of the cilia-like photocatalyst (Fig. 3C). Photocatalysts also can be reused several times and remain active without significant performance change.

Catalytic micromotors demonstrated enhanced degradation of model pollutants by reactive species due to the micromixing capability of the catalytic system.[17–19] However, only very recently, titania thin films and particles were used as active components of micromotors[16,20] and micropumps.[21]

Giudicatti *et al.* described a method to fabricate rolled up TiO_2 microtubes (Fig. 3D), which can swim under UV light irradiation (Fig. 3E and F).[16] Tubular motors show a clear enhanced motion under light as seen in the tracking trajectories of Fig. 3E (no light) *vs.* Fig. 3F (UV light on) and the Mean Square Displacement. Diffusiophoresis could be the possible mechanism behind the self-propulsion of these motors. In their fabrication method, first a sacrificial layer was prepared by photolithography of polymers on a glass or silicon substrate. Different sizes of patterns were transferred onto the samples using exposure of UV light by a mask aligner. Then, TiO_2 nano-membranes were deposited at an angle of 15° with different deposition rates *via* an e-beam evaporator under an oxygen environment. After rolling up of the nano-membranes, TiO_2 microtubes were dried and annealed to achieve anatase structure. It is expected that other types of motors will use photocatalytic reactions with the aim of finding clean fuels.

Developing effective photocatalytic systems is the key to harvest clean and inexpensive energy from the sun. Recent advances in photocatalysis have shown to be promising approaches for future technologies of electricity production and environmental remediation. Design and fabrication of forthcoming nano-photocatalysts incorporating advanced properties like self-propelled motion and micromixing features, full spectrum photo-activity, improved light absorption and integration in optofluidic systems have great potential to enhance solar energy harvesting capacity in compact devices.

Acknowledgements

The authors acknowledge the European Research Council under the European Union's Seventh Framework Programme (FP7/2007-2013)/ERC Grant Agreement 311529 (Lab-in-a-tube and Nanorobotics biosensors). L.S. acknowledges the Beatriu de Pinós Program for financial support through project no. 2013 BP-B 00007. This work was supported by a National Research Foundation of Korea (NRF) grant funded by the Korean Government (MEST) (2008-0061983).

Notes and references

1 R. A. Maurya, K.-I. Min and D.-P. Kim, *Green Chem.*, 2014, **16**, 116–120.
2 N. Wang, X. Zhang, Y. Wang, W. Yu and H. L. W. Chan, *Lab Chip*, 2014, **14**, 1074–1082.
3 S. S. Ahsan, A. Gumus and D. Erickson, *Lab Chip*, 2013, **13**, 409–414.
4 Z. Meng, X. Zhang and J. Qin, *Nanoscale*, 2013, **5**, 4687–4690.
5 L. Li, G. Wang, R. Chen, X. Zhu, H. Wang, Q. Liao and Y. Yu, *Lab Chip*, 2014, **14**, 3368–3375.

6 C.-T. Dinh, H. Yen, F. Kleitz and T.-O. Do, *Angew. Chem., Int. Ed.*, 2014, **53**, 6618–6623.
7 J. I. L. Chen, G. von Freymann, S. Y. Choi, V. Kitaev and G. A. Ozin, *Adv. Mater.*, 2006, **18**, 1915–1919.
8 Y. Sang, Z. Zhao, M. Zhao, P. Hao, Y. Leng and H. Liu, *Adv. Mater.*, 2015, **27**, 363–369.
9 G. Yin, M. Nishikawa, Y. Nosaka, N. Srinivasan, D. Atarashi, E. Sakai and M. Miyauchi, *ACS Nano*, 2015, **9**, 2111–2119.
10 R. Kuriki, K. Sekizawa, O. Ishitani and K. Maeda, *Angew. Chem., Int. Ed.*, 2015, **54**, 2406–2409.
11 Z. Gan, X. Wu, M. Meng, X. Zhu, L. Yang and P. K. Chu, *ACS Nano*, 2014, **8**, 9304–9310.
12 K. Akatsuka, G. Takanashi, Y. Ebina, N. Sakai, M.-A. Haga and T. Sasaki, *J. Phys. Chem. Solids*, 2008, **69**, 1288–1291.
13 K. Maeda, K. Sekizawa and O. Ishitani, *Chem. Commun.*, 2013, **49**, 10127–10129.
14 P. A. Anderson, G. B. Deacon, K. H. Haarmann, F. R. Keene, T. J. Meyer, D. A. Reitsma, B. W. Skelton, G. F. Strouse and N. C. Thomas, *Inorg. Chem.*, 1995, **34**, 6145–6157.
15 D. Zhang, W. Wang, F. Peng, J. Kou, Y. Ni, C. Lu and Z. Xu, *Nanoscale*, 2014, **6**, 5516–5525.
16 S. Giudicatti, S. M. Marz, L. Soler, A. Madani, M. R. Jorgensen, S. Sanchez and O. G. Schmidt, *J. Mater. Chem. C*, 2014, **2**, 5892–5901.
17 L. Soler, V. Magdanz, V. M. Fomin, S. Sanchez and O. G. Schmidt, *ACS Nano*, 2013, **7**, 9611–9620.
18 L. Soler and S. Sanchez, *Nanoscale*, 2014, **6**, 7175–7182.
19 W. Gao and J. Wang, *ACS Nano*, 2014, **8**, 3170–3180.
20 J. Li, V. V. Singh, S. Sattayasamitsathit, J. Orozco, K. Kaufmann, R. Dong, W. Gao, B. Jurado-Sanchez, Y. Fedorak and J. Wang, *ACS Nano*, 2014, **8**, 11118–11125.
21 Y. Hong, M. Diaz, U. M. Córdova-Figueroa and A. Sen, *Adv. Funct. Mater.*, 2010, **20**, 1568–1576.